available at www.sciencedirect.com

ScienceDirect

journal homepage: www.elsevier.com/locate/ijggc

Carbon dioxide storage potential of shales

Andreas Busch [a,1,*], *Sascha Alles* [a], *Yves Gensterblum* [a], *Dirk Prinz* [a], *David N. Dewhurst* [b], *Mark D. Raven* [c], *Helge Stanjek* [d], *Bernhard M. Krooss* [a]

[a] *RWTH Aachen University, Institute of Geology and Geochemistry of Petroleum and Coal, Lochnerstr. 4-20, D-52056 Aachen, Germany*
[b] *CSIRO Petroleum, Australian Resources Research Centre, Western Australia, Australia*
[c] *CSIRO Land and Water, Urrbrae, South Australia, Australia*
[d] *RWTH Aachen University, Clay and Interface Mineralogy, Aachen, Germany*

ARTICLE INFO

Article history:
Received 15 June 2007
Received in revised form
14 February 2008
Accepted 7 March 2008
Published on line 24 April 2008

Keywords:
CO_2 storage
Cap rocks
CO_2 sorption
CO_2 diffusion
Sealing integrity

ABSTRACT

Options for the geologic storage of carbon dioxide vary from saline aquifers and depleted oil and gas reservoirs to unminable coal seams and abandoned coal mines. Important aspects include the sealing integrity of the cap rock and potential changes in this integrity, owing to the interaction with CO_2.

In this study, diffusive transport and gas sorption experiments on one well characterised shale sample (Muderong Shale, Australia) and different clay minerals were performed to obtain information on the sealing integrity and the CO_2 storage potential of these materials. All measurements were performed under reservoir conditions relevant for CO_2 storage (T = 45–50 °C; $p < 20$ MPa). Repeat diffusion experiments on one shale plug yielded increased effective diffusion coefficients and a decrease in the concentration of the bulk CO_2 volume in the sample. The latter is believed to be dissolved in formation water, sorbed to mineral surfaces or involved with geochemical reactions. For the Muderong Shale, bulk volume CO_2 concentrations are greater within the experimental time frame (222–389 mol/m^3), when compared to coal and cemented sandstone (3–4 and 8–10 mol/m^3), respectively. This high CO_2 storage potential could not fully be explained by CO_2 dissolution in water alone. Thus, gas sorption experiments were performed on crushed shale and various clay minerals. High CO_2 sorption capacities (e.g. up to 1 mmol/g for the Muderong Shale) show that the high CO_2 concentration is related to a combination of CO_2 dissolution in water and gas sorption on clay minerals.

Additionally, changes in specific surface areas before and after the sorption experiments and variations in the CO_2 sorption and diffusion behaviour due to repetitive experiments on the identical sample were observed, possibly related to geochemical alteration of the Muderong Shale and the clay minerals. These could not be quantified however and seemed to occur only at high pressures.

Results obtained in this study provide a more positive view on the sealing integrity of intact cap rock formations. Carbon dioxide that migrates from a storage reservoir into the cap rock through the pore network will be immobilised to a certain extent, hence minimising (slow, diffusion-driven) leakage and providing additional CO_2 storage potential.

* *Corresponding author*. Tel.: +49 241 8098293; fax: +49 241 8092152.
E-mail address: busch@lek.rwth-aachen.de (A. Busch).
[1] Present address: Shell International Exploration and Production B.V., Kessler Park 1, 2288 GS Rijswijk, The Netherlands.
E-mail: busch_a@web.de
1750-5836/$ – see front matter
doi:10.1016/j.ijggc.2008.03.003

1. Introduction

In recent years, research in subsurface CO_2 storage in geological formations has increased rapidly. The main focus has been to lower anthropogenic CO_2 emissions which are believed to be a major factor contributing to global warming. Some favoured storage options are saline aquifers, depleted gas and oil reservoirs or unminable coal seams (Bachu et al., 1994; Freund and Ormerod, 1997; Holloway, 1997; Hitchon et al., 1999; Bachu, 2000).

Studies cover issues such as gas–water–rock interactions, multiphase flow, reservoir engineering and modelling, and monitoring and verification. A common aspect of all CO_2 capture and storage (CCS) options is the sealing efficiency of cap rocks above potential CO_2 storage reservoirs. The quantitative assessment of leakage risks and leakage rates is a prerequisite for site approval, public acceptance and the awarding of credits for stored CO_2 quantities.

Leakage through caprocks may occur in three ways: (i) rapid (''catastrophic'') leakage by seal-breaching (mechanical failure) or damage of well casing (corrosion of pipes and cements), resulting in gas flow through a (micro-) fracture network, (ii) long-term leakage controlled by capillary sealing efficiency (e.g. Hildenbrand et al., 2004; Al-Basali et al., 2005; Chiquet et al., 2005) and permeability (after capillary breakthrough pressure is exceeded) and (iii) diffusive loss of dissolved gas through water-saturated pore space.

Molecular diffusion of CO_2 is characterised by a low transport capacity, but it is a continuous and ubiquitous process. However, rather than causing substantial gas loss, the process is the rate-controlling step of mineral reactions, associated with seal alteration and sorption processes. Few data are available on the diffusive transport of CO_2 in geologic seals.

Prior research on molecular gas transport through cap rocks mainly focused on hydrocarbon loss from natural gas reservoirs (e.g. Krooss and Leythaeuser, 1988, 1996, 1997; Krooss and Schäfer, 1987; Krooss et al., 1992a,b; Leythaeuser et al., 1980; Montel et al., 1993; Nelson and Simmons, 1992, 1995). Krooss et al. (2003) reported CO_2 diffusion parameters of samples from different lithotypes (coal, cemented sandstones, shales). Their results indicated that shales are capable of storing significant amounts of CO_2 dissolved in formation fluids, trapped by mineral reactions or sorbed to organic compounds or mineral surfaces. Additional investigations are reported here for CO_2 sorption and diffusion behaviour of selected shale samples and clay mineral standards (Ca-rich montmorillonite, Na-rich montmorillonite, kaolinite, illite).

In this study CO_2 sorption and diffusion measurements have been performed in order to assess the molecular transport through and the sorptive storage behaviour of a well-defined regional caprock and a variety of clay minerals. This has been done partly in a repetitive succession on the identical sample material to obtain insight into the changes in diffusion and sorption behaviour due to the interaction with CO_2-enriched waters.

2. Sample description

The Muderong Shale of Cretaceous age is the regional top seal in the Carnarvon Basin on the Northwest Shelf of Australia. The sample is from a depth of 1454 m below seafloor (mbsf). The shale was partially dried out when recovered and was preserved under light process oil from the recovery point onwards to prevent further desiccation. XRD analysis shows that this shale is dominantly interstratified illite–smectite, kaolinite and quartz (Table 1). It has a porosity of ~20% and a 2.33 g/cm^3 bulk density (determined by weighing and drying), a moderately high specific surface area of 25 m^2/g (by nitrogen adsorption/desorption) and a cation exchange capacity of 0.24 mequiv./100 g in agreement with its clay-rich mineralogy (Table 1). Pore size distributions (by mercury porosimetry, Dewhurst et al., 2002a) indicate capillary threshold pressures of ~48 MPa (Kovack et al., 2004). Scanning electron microscope (SEM) examination shows that the Muderong Shale is a relatively uniform (non-laminated), fissile shale, with clay matrix (Fig. 1a and b). Preferential particle orientation of rigid grains and clay matrix is observed, although the clay matrix orientation can be affected locally by the presence of more rigid particles (Fig. 1c). Pyritisation of foraminifers occurs along with precipitation of early diagenetic kaolinite (Fig. 1b and c) and siderite (Fig. 1d). Further details of the analytical methods and the composition, physical and mechanical properties of the Muderong Shale were reported by Dewhurst et al. (2002a,b) and Dewhurst and Hennig (2003).

Table 1 – Properties and mineralogy of Muderong Shale

Grain density (g/cm^3)	2.70
Bulk density (g/cm^3)	2.33
Porosity (m^3/m^3)	0.20
Specific surface area (m^2/g)	25.0
Cation exchange capacity (mequiv./100 g)	0.24
Capillary entry pressure (Air–Hg, MPa)	48.3
Total organic carbon (%)	<0.5
Clay content (g/g)	0.66
Clay fraction (g/g)	0.45
Mineral composition	**Content (g/g)**
Illite–smectite	0.27
Smectite in I-S	0.20
Mica/illite	0.08
Kaolinite	0.26
Chlorite	0.05
Quartz	0.27
Siderite	0.02
Orthoclase	0.03
Pyrite	0.02

Ca-rich montmorillonite (STx-1b), Na-rich montmorillonite (SWy-2), illite (Imt-1) and kaolinite (KGa-1b) used in this study were obtained from the The Clay Minerals Society (http://www.clays.org/) Source Clays Repository (Purdue University, Indiana, USA). These samples were described in detail by Costanzo and Guggenheim (2001).

For the sorption experiments different moisture states have been used: either the samples were used as received (a.r.) or they were used dry. The latter has been achieved by drying the samples under vacuum at 105 °C for >90 min in the sample cell in order not to bring the sample in contact with atmospheric humidity.

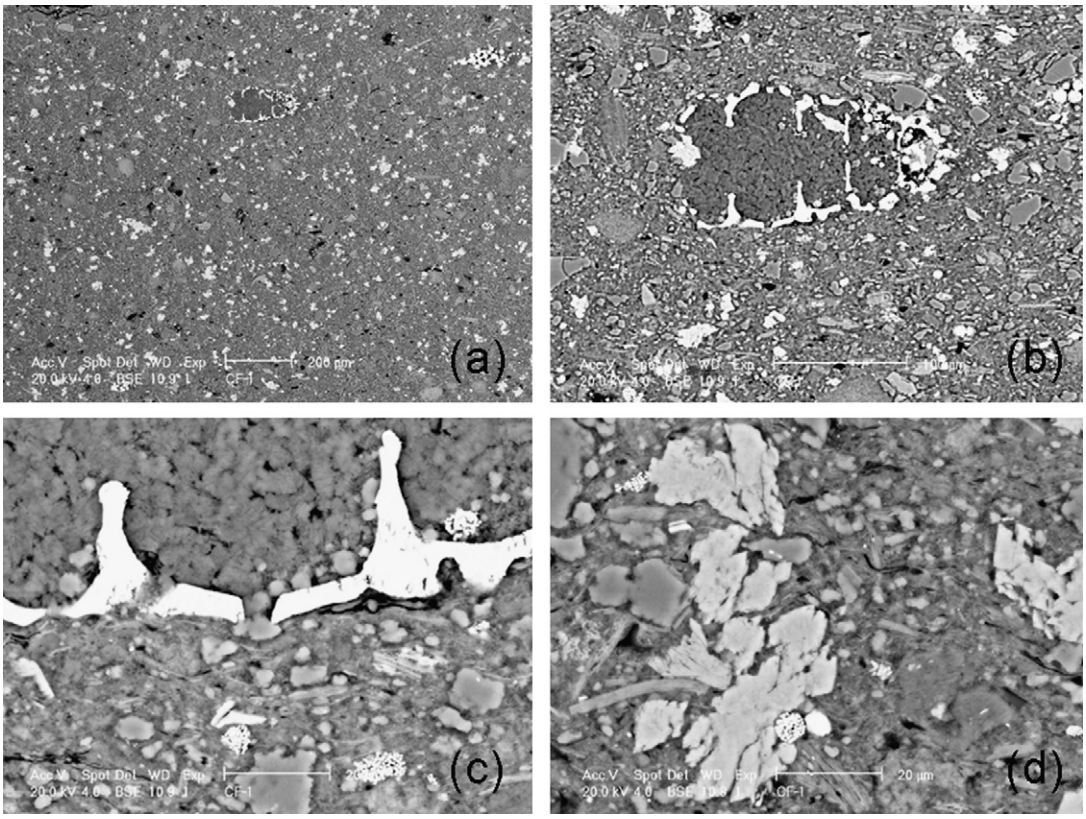

Fig. 1 – Backscattered scanning electron microscope images of the Muderong Shale sample: (a) low magnification image showing the fine-grained nature (most particles <50 μm diameter); (b) magnified from (a), showing pyritised foraminifera infilled with clay; (c) high magnification of (b) reveals the foram test is infilled with vermicular kaolinite that has been protected from compaction, enhanced compaction of clays around the foram and small pyrite framboids (bright); (d) high magnification image showing siderite (bright), a small pyrite framboid, tightly compacted clay fabric and fine-grained quartz particles (larger, grey grains).

3. Experimental methods

3.1. *Diffusion experiments*

Carbon dioxide diffusion experiments were conducted in triaxial flow cells constructed for confining pressures and axial loads of up to 50 MPa, with temperatures up to 350 °C. The cylindrical sample plugs have a diameter of 28.5 mm and range in length from 5 to 20 mm which is usually chosen to keep the experimental time frame reasonable. The plug is placed between two porous stainless-steel disks (Fig. 2) and the assembly is mounted between two stainless-steel pistons with boreholes for fluid introduction and removal. To prevent leakage and diffusion, the outer surface of the sample/piston arrangement is sealed with a double-layered sleeve. The inner sleeve consists of lead foil (0.25 mm thickness); for the outer layer, a thin-walled copper tube is used. Confining pressures are kept higher than fluid pressure to avoid fracturing of the sample.

Prior to the diffusion experiments, the conductive pore system of the samples is water-saturated with tap water by applying pressures of up to 8 MPa on one side. The resulting flow rate at the downstream side is monitored to determine the permeability coefficient. Subsequently, both sides of the flow cell are pressurised with water up to the pressure level chosen for the diffusion experiment. The diffusion experiment is initiated by displacing the water in the lower side of the flow cell by CO_2. This has been done at 50 °C experimental temperature and an effective fluid pressure of 6–7 MPa (Fig. 2). A communicating tubing system ensures that there is no

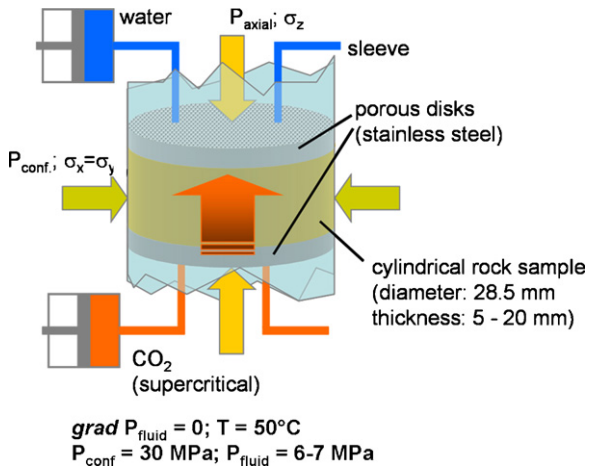

Fig. 2 – Schematic diagram of the CO_2 diffusion experiment under controlled effective stress conditions.

pressure gradient (volume flow) between top and bottom chamber of the measuring cell.

Schlömer and Krooss (2004) describe the flow scheme of the experimental set-up with the peripheral valve and tubing system used here. The diffused gas is collected in the top chamber of the flow cell for 1–2 h and then transferred to a purge and trap system. Here, CO_2 is stripped from the water by a helium gas flow and adsorbed on a molecular sieve trap. In a subsequent step the trapped CO_2 is mobilised thermally and transferred to the gas chromatograph (GC) for quantification with a thermo-couple detector (TCD).

The diffusion experiments are conducted as non-steady-state measurements, i.e. the diffusive breakthrough of the gas is monitored and evaluated to yield the effective diffusion coefficient and the equilibrium bulk rock volume CO_2 concentration at the gas/rock interface in the bottom chamber. A detailed description of the determination of effective diffusion coefficients and the derivation of diffusion equations was given by Schlömer and Krooss (2004). A short outline is provided in Appendix A.

3.2. *Sorption experiments*

3.2.1. *High-pressure sorption experiments*

In high-pressure sorption experiments (ambient pressure up to 25 MPa), the gas sorption capacity (sorption isotherms) of powdered sample material is determined as a function of pressure by a manometric method. Fig. 3 shows a schematic illustration of the experiment set-up which consists of a stainless-steel sample cell, a set of actuator-driven valves and a high-precision pressure transducer (max. pressure 16 MPa), with a precision of 0.05% of the full-scale value. The volume between valves 2 and 3, including the void volume of the pressure transducer, is used as a reference volume which is calibrated initially by helium pycnometry. The powdered shale samples are placed in a stainless-steel sample cell. A 2-μm filter-disc is used to prevent mineral particles from entering the valves.

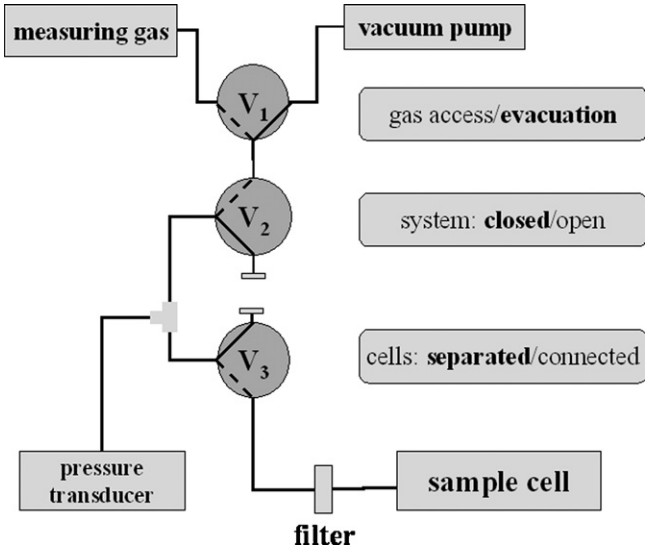

Fig. 3 – Schematic diagram for single component gas adsorption on shale and clay samples. The volume between V2 and V3, including dead volume of the pressure transducer, is used as reference volume.

The experimental device is located in a temperature-controlled oven to ensure a constant temperature (±0.1 °C) in all experiments. Single-gas sorption experiments were performed at 45 and 50 °C. At these temperatures CO_2 is either in the gaseous or, at pressures above p_c, in the supercritical state (T_c = 30.95 °C; p_c = 7.38 MPa).

A detailed description of the method was given by Krooss et al. (2002), Busch et al. (2003, 2004, 2007), and Siemons and Busch (2007). The experimental data are evaluated in terms of excess (Gibbs) sorption isotherms. Here the observed reduction in gas pressure resulting from gas sorption is compared to the theoretical "non-sorption" case. The volume changes relating to the increased amount of adsorbed phase with pressure are not considered.

3.2.2. *Low-pressure nitrogen sorption experiments*

To detect structural changes in the pore system of the clay minerals, specific surface area measurements were performed on as received Ca-rich montmorillonite, Na-rich montmorillonite and kaolinite samples before and after high-pressure sorption experiments with supercritical CO_2. Specific surface areas were determined by low-pressure nitrogen sorption on the dry material with a Micromeritics GEMINI 2360 instrument using the BET method (Brunauer et al., 1938). The measurements were performed at liquid nitrogen temperature (−196 °C) up to a final pressure of 0.126 MPa. Due to the low-pressures used, no correction for non-ideal behaviour of the gas was made.

Clay samples were evacuated and kept in a vacuum (<1 Pa) at 105 °C for at least 6 h. The vacuum oven was then vented with helium and the sample cells (quartz) were closed while the samples were still under a helium atmosphere. Until used, the dry samples were stored in a desiccator under helium.

4. Results

Permeability tests conducted with the Muderong Shale prior to the first diffusion experiments yielded permeability coefficients of $\sim 10^{-21}$ m^2 (1 nDarcy) (Fig. 4). These values are relatively low compared to permeability coefficients commonly observed for moderately compacted shales.

4.1. *Diffusion experiments*

The experimental diffusion curves (data points and best fits) obtained from diffusion experiments on the Muderong Shale sample plug are shown in Fig. 5 (Experiment 1) and Fig. 6 (Experiment 2). The cumulative amounts (Q) of CO_2 diffused axially through the cylindrical sample plug per unit cross-section area (units of Q: mmol/m^2) are plotted as a function of time (t in h) elapsed since the start of the experiment. The slopes of the tangents to the curves represent the steady-state flux (mmol/m^2/h). The diagrams indicate the lag times (t_0), defined as the intersection of the tangent to the steady-state diffusion curve with the x-axis, and the Q_0-values the intercept of the tangent with the y-axis. These two characteristic parameters of the diffusion curve are used to derive the effective diffusion

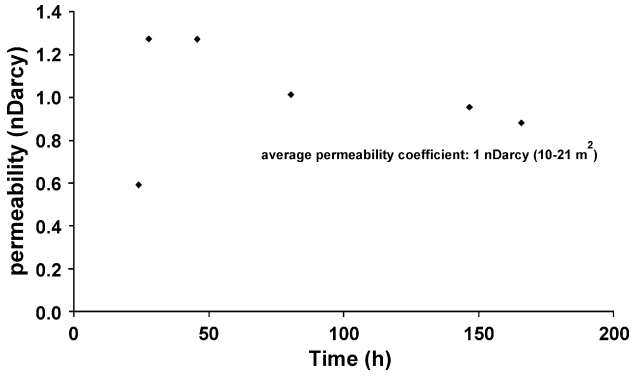

Fig. 4 – Water permeability measurement on Muderong Shale plug prior to first CO_2 diffusion experiment.

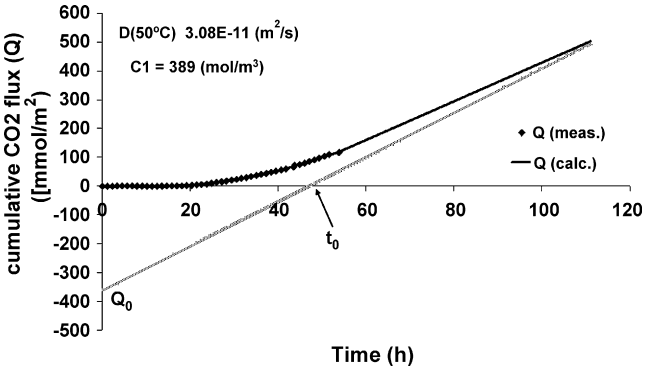

Fig. 5 – Cumulative CO_2 diffusion curve from Experiment 1 on Muderong Shale plug at 50 °C.

coefficient (D) and the gas storage capacity (C_1) of the samples (cf. Krooss and Schäfer, 1987). Experiment 1 was terminated before steady-state flow was reached. However a fit of the diffusion function to the experimental data provided a reasonable estimate of the diffusion parameters.

Table 2 summarizes the effective diffusion coefficients and C_1-values of these two experiments. Effective diffusion coefficients of 3.08 and 4.81×10^{-11} m^2/s were obtained for Experiments 1 and 2, respectively. The C_1-values (Experiment 1, 389 mol/m^3; Experiment 2, 222 mol/m^3) denote the bulk volume concentration (mol/m^3 shale) of CO_2 within the rock sample at the gas/shale interface.

4.2. *Sorption experiments*

4.2.1. *High-pressure CO_2 experiments*

Fig. 7 shows the excess sorption isotherms for the Muderong Shale measured at 50 °C with an as received (a.r.) water content of 3.34% and in the dry state. The a.r. shale has a lower water content than expected probably as a result of poor sample preservation and thus is not fully saturated to its natural state. For the a.r. shale, two measurements were performed on the identical sample to investigate reproducibility. The shape of the isotherm differs significantly from "normal" gas sorption isotherms and can be separated into three parts: (1) pressure from 0 to ~7 MPa: excess sorption shows a near linear trend for each isotherm. This trend is

Table 2 – Effective diffusion parameters for Muderong Shale

	t_0 (s)	Q_0 ($mmol/m^2$)	D_{eff} (m^2/s)	C_1 (mol/m^3)
Experiment 1	1.69×10^5	−363	3.08×10^{-11}	389
Experiment 2	1.09×10^5	−207	4.81×10^{-11}	222

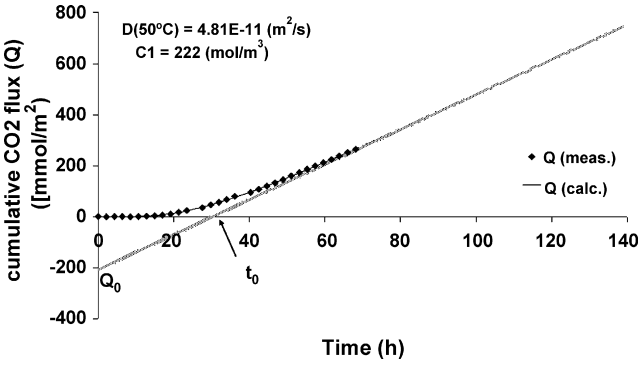

Fig. 6 – Cumulative CO_2 diffusion curve on Muderong Shale plug at 50 °C (Experiment 2).

similar for each experiment indicating no effect of water content; (2) pressure from 7 to ~12 MPa: excess sorption shows a steep increase for untreated shale (first run a.r.) and an initial decrease for the other two experiments (second run a.r. and dry), followed by a similar peak as for the untreated shale. The maximum sorption capacity varies for the three samples and decreases from the untreated (first run a.r.) to the dry sample from ~1.0 to ~0.4 mmol/g. (3) above 12 MPa, all isotherms show a parallel and continuous decrease in excess sorption capacity with pressure.

The CO_2 sorption isotherms of the a.r. and dry clays, measured at 45 °C, generally differ from those of the shale. Four different samples were tested either with a.r. moisture content or in the dry state (Fig. 8). For each sample, the dry measurements yielded higher excess sorption values than the corresponding a.r. samples. The highest sorption capacities were obtained for Ca-rich montmorillonite with maximum values of ~1.65 and ~1.3 mmol/g for the dry and the a.r.

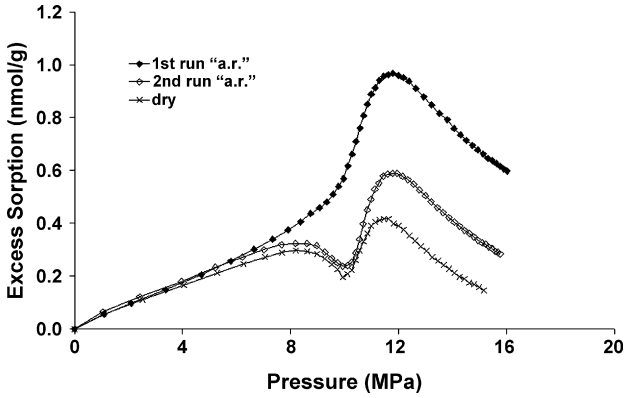

Fig. 7 – CO_2 excess sorption experiment on Muderong Shale at 45 °C.

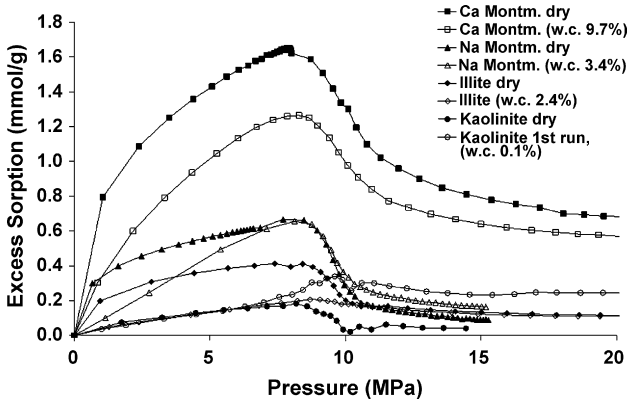

Fig. 8 – CO_2 excess sorption experiments on various samples containing mostly Ca-rich montmorillonite, Na-rich montmorillonite, illite, kaolinite in the dry and as received moisture state (water contents are given in the legend).

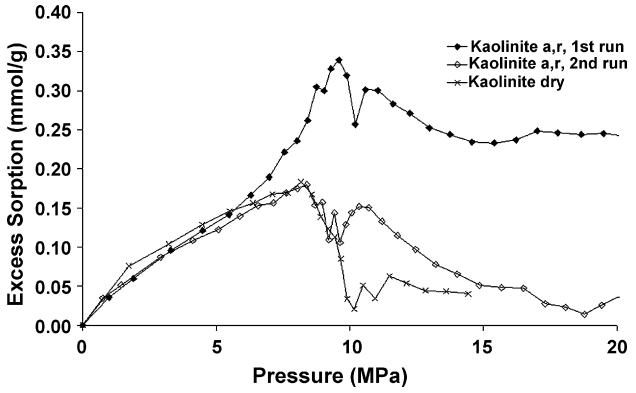

Fig. 9 – CO_2 excess sorption experiments on sample containing a.r. kaolinite.

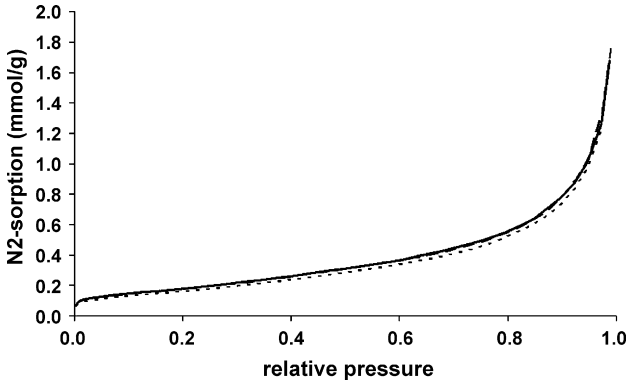

Fig. 10 – Nitrogen sorption isotherms for original Muderong Shale and samples exposed to CO_2 (solid line = original sample; long-dashed line = dry sample short-dashed line = moist sample after exposure to CO_2).

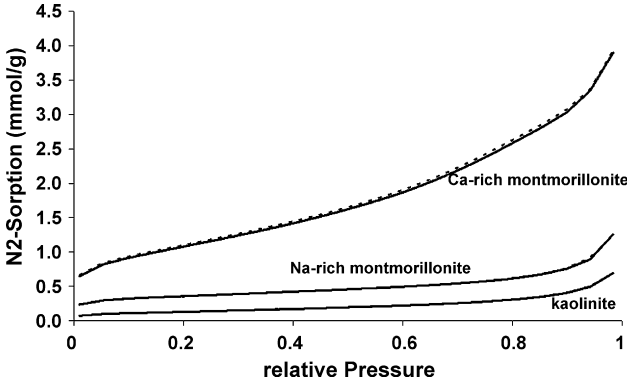

Fig. 11 – Nitrogen sorption isotherms (BET) for original clay minerals and samples exposed to CO_2 (solid lines = original samples; dashed lines = samples after exposure to CO_2).

sample, respectively. The lowest sorption values, however, were found for kaolinite and illite with maximum values <0.4 mmol/g.

The shape of the CO_2 sorption curves on kaolinite differed from those obtained for the other clay minerals (Fig. 9). The isotherms show fluctuations at pressures above 8–10 MPa. Furthermore, the a.r. measurement (first run, Fig. 9) shows a sorption peak similar to the one observed for the Muderong Shale. A re-run with CO_2 was performed on the same sample to test for reproducibility (second run, Fig. 9). It is obvious that the two isotherms are very similar up to ~8 MPa. At higher pressures, however, the second a.r. isotherm shows significantly lower sorption capacities that are similar to the dry measurement in Fig. 7. The same was observed for the Muderong Shale (Fig. 7).

4.3. *Low-pressure N_2 sorption experiments*

Low-pressure N_2 sorption experiments were performed on the Muderong Shale (a.r. and dry, Fig. 10) and on three a.r. clay

Table 3 – Comparison of BET specific surface areas of clay minerals and Muderong Shale before and after CO_2 treatment

Sample	SSA before treatment (m^2/g)	SSA after CO_2 treatment of moist sample (m^2/g)	SSA after CO_2 treatment of dry sample (m^2/g)
Muderong Shale	14.6	13.1	14.5
Ca-rich montmorillonite	92.3	94.1	n.a.
Na-rich montmorillonite	28.0	28.3	n.a.
Kaolinite	11.3	11.1	n.a.
Illite	n.a.	n.a.	n.a.

minerals (Ca-rich montmorillonite, Na-rich montmorillonite, kaolinite, Fig. 11). No differences larger than the expected experimental error (~3–4%) in the N_2 sorption isotherms or specific surface areas (SSA) were observed for the minerals (Table 3). The CO_2-treated a.r. Muderong Shale however showed a decrease in SSA from 14.6 to 13.1 m^2/g as compared to the initial a.r. sample. There was no change in SSA observed between CO_2-treated and untreated dry Muderong Shale.

5. Discussion

5.1. CO_2 diffusion in the Muderong Shale

The CO_2 diffusion coefficients obtained from the Muderong Shale in successive tests are of the same magnitude, the value from Experiment 2 being slightly higher than from Experiment 1 (Figs. 5 and 6). This may result from chemical alteration of the conducting pore network during the initial experiment (Experiment 1), possibly related to mineral reactions. Effective diffusion coefficients of gases in water-saturated rocks are also affected by sorption processes as indicated in diffusion experiments of methane in shales with different organic matter contents (Zhang and Krooss, 2001). Thus, the elevated and partly irreversible sorption of CO_2 may have retarded the diffusion front in the Muderong Shale diffusion experiment (first run) while the interaction of the shale with CO_2 was probably lower in Experiment 2, as indicated from the lower C_1-value.

Further systematic tests are in progress to provide more insight into the natural variability of diffusion coefficients and changes due to CO_2–water–rock interactions.

Diffusion coefficients of CO_2 in water as reported by Gertz and Loeschcke (1956) and Vivian and King (1964) are between 2 and 3×10^{-9} cm^2/s (at 37 °C). As discussed by Krooss et al. (1992a), the relationship

$$D_{\text{eff}} = \frac{D_{\text{aq}}}{\tau} \quad (1)$$

where D_{eff} denotes the effective diffusion coefficient and D_{aq} is the diffusion coefficient in the pore water, allows the estimation of nominal tortuosity (τ) of the shale pore system. For the Muderong Shale, this tortuosity value is approximately 40–70.

The C_1-values obtained from the diffusion experiments are a measure of the specific CO_2 storage capacity of the shale at the pressure/temperature conditions of the experiment. Evidently, the C_1-value decreased from 389 in the first to 222 mol/m^3 in the second test (cf. Figs. 5 and 6). The significant decrease in CO_2 storage capacity in diffusion Experiment 2 is attributed to irreversible storage of CO_2 in Experiment 1, e.g. by mineral reactions. For comparison, Table 4 lists the CO_2 diffusion parameters of the Muderong Shale, a Carboniferous coal, and cemented sandstone. The Muderong Shale exhibits the lowest diffusion coefficients and the highest CO_2 storage capacity (C_1-values). The steady-state diffusive flux, which is controlled both by the effective diffusion coefficient and the "solubility" or storage capacity of the gas in the water-saturated rock, is also much larger for the Muderong Shale than for the other two samples.

5.2. CO_2 sorption on shales and clay minerals

In the high-pressure sorption experiments the a.r. Muderong Shale showed a higher CO_2 sorption capacity than in the dry state (Fig. 7). This behaviour was unexpected because water and CO_2 are believed to compete for the same sorption sites, which should result in lower CO_2 sorption capacities for moist samples. For the montmorillonite and illite samples investigated, substantially higher sorption capacities were observed with the dry samples whereas the a.r. kaolinite exhibited higher CO_2 sorption capacities than the dry clay at pressures above 7 MPa (Fig. 9). The drying procedure was the same in all cases and therefore any structural rearrangements would be expected for both, the clays and the shale samples. Further one would also expect that deviations over the entire pressure range of the sorption isotherms will occur. This is not the case, because for all measurements performed on the Muderong Shale, the sorption behaviour is similar at pressures up to ~7 MPa.

Repeat sorption tests on the a.r. Muderong Shale and kaolinite samples showed a decrease in sorption capacities, especially at elevated pressures. These repeat measurements demonstrated sorption behaviour similar to the corresponding dry measurements.

Although numerous CO_2 sorption measurements on coals under various conditions have been published, reports on sorption isotherms on shales at high pressures are sparse. Nuttall et al. (2005) investigated carbonaceous Devonian black gas shales from Kentucky, USA and the CO_2 storage and methane recovery potential ($T = 30$ °C, $p < 5.5$ MPa for CO_2 and <10 MPa for CH_4, respectively). They found a direct positive

Table 4 – Comparison of effective CO_2 diffusion parameters measured on a coal, a cemented sandstone and the Muderong Shale

	Sample					
	Coal BRZ 405		Cemented sandstone		Muderong Shale	
	Coal 1 (45 °C)[a]	Coal 2 (45 °C)[a]	ss 1 (50 °C)[a]	ss 2 (50 °C)[a]	sh 1 (50 °C)[a]	sh 2 (50 °C)[a]
D_{eff} (m^2/s)	1.43×10^{-9}	1.18×10^{-9}	2.61×10^{-10}	1.89×10^{-10}	3.08×10^{-11}	4.81×10^{-11}
C_1 (mol/m^3)	3.30	4.14	9.8	8.3	389	222
Steady-state flux ($mmol/m^2/h$)	0.93	1.0	0.73	0.45	7.62	6.9

[a] Experiment (temperature).

correlation between CO_2 storage capacity and total organic carbon (TOC) whereas no correlation with the clay mineral content was observed.

Volzone and co-authors investigated the sorption behaviour of montmorillonite and kaolinite for CO_2, CO, N_2, CH_4 and SO_2 (Volzone and Ortiga, 2000, 2006; Volzone et al., 2002, 2006; Venaruzzo et al., 2002; Melnitchenko et al., 2000). These measurements are usually performed at 0.1 MPa and 25 °C, thus not representing reservoir conditions for CO_2 storage. However, at these *pT* experimental conditions, significant sorption capacities for different clay minerals were observed with maximum values for $SO_2 > CO_2 > CH_4 \geq N_2$: $0.66 > 0.24 > 0.08 \geq 0.07$ mmol/g. The mechanisms leading to gas sorption on clay minerals are not well studied. For example Venaruzzo et al. (2002) found a correlation between CO_2 sorption and BET surface areas and micropore volume of clays. A similar phenomenon was observed in this study: BET surface areas, as measured with N_2 (Chlou and Rutherford, 1993), decrease in the order montmorillonite > illite > kaolinite and this is the same trend as observed for the sorption capacity. These observations seem to support physical surface sorption as reported for various other porous materials, for example for activated carbons, coals or polymers.

5.3. *CO_2 storage potential of shales*

The C_1-values obtained from the diffusion experiments provide information on the bulk storage capacity of shales at the experimental *pT* conditions. Given sufficient time, an equilibrium concentration of CO_2 will be established in the pore water at the interface of the water-saturated shale and the free CO_2 phase. If no adsorption occurs (i.e. CO_2 resides exclusively in the pore water), then C_1 corresponds to the product of the aqueous solubility of CO_2 (C_{aq}) under experimental conditions and porosity (Φ)

$$C_1 = C_{aq}\Phi \quad (2)$$

Any higher observed C_1-value is related to sorption or mineral-reaction effects. The solubility of CO_2 in pure (salt-free) water at the experimental conditions can be estimated by the relationship of Duan and Sun (2003). At 50 °C and pressures between 6 and 7 MPa, the solubility of CO_2 in (salt-free) water is between ~870 and 960 mol/m^3 H_2O (cf. Fig. 12). Assuming a porosity of 20% for the Muderong Shale (Table 1), the bulk volume CO_2 concentration is determined at ~170–190 mol/m^3 for non-sorption and assuming equilibrium of CO_2 and pore water. Thus, the significantly higher C_1-values (222–389 mol/m^3 Figs. 5 and 6) derived from the diffusion experiment indicate significant CO_2 sorption (on organic matter and minerals) or mineral reactions in the shale. This value for the combined sorption/mineral-reaction potential, at the first contact of CO_2 with the shale, may be as much as 200 mol/m^3 (0.086 mmol/g). The C_1-value in Experiment 2 (222 mol/m^3, Fig. 6) is lower than in Experiment 1 (389 mol/m^3, Fig. 5). This variance indicates that irreversible sorption/reaction of CO_2 occurred during Experiment 1 (cf. Figs. 7 and 8).

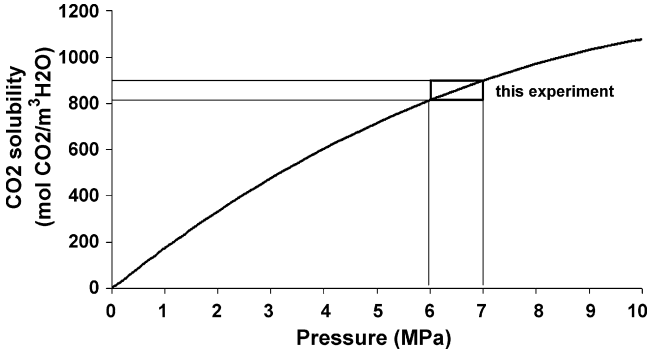

Fig. 12 – CO_2 solubility in water at 50 °C assuming zero NaCl concentration calculated after Duan and Sun (2003).

The sorption measurements on clay minerals show that the CO_2 sorption capacity of Muderong Shale may be attributed entirely to its clay minerals constituents. Sorption on organic matter is assumed to play a minor role, taking into account the low TOC of the Muderong Shale (<0.5%). From sorption experiments on coal it is well known that 0.5% TOC can only sorb limited amounts of CO_2 (e.g. Krooss et al., 2002).

Although mineral reactions might have occurred, these C_1-values can fully be explained by pure sorption as has been verified in Fig. 7. When directly comparing diffusion and sorption tests, it shows that less CO_2 gets sorbed, dissolved or trapped by mineral reactions in the diffusion measurements (222–389 mol/m^3 corresponding to ~0.10–0.17 mmol/g) than in the sorption tests (0.25–0.3 mmol/g) at comparable pressures (6–7 MPa). It is likely that during the diffusion experiments, full equilibration of the sample plug was not achieved, i.e. not all sorption sites were reached.

Additional mineral reactions that are dependent on the timeframe of the experiment could again increase the C_1-value of the shale, leading to an even higher CO_2 storage potential. In recent years CO_2–water–rock interactions in geological storage formations have experienced increased attention (e.g. Gunter et al., 1993, 2000; Kaszuba et al., 2003, 2005; Emberley et al., 2004; Brosse, 2005a,b; Rosenbauer et al., 2005; Shiraki and Dunn, 2000; Gaus et al., 2005; Knauss et al., 2005; Bertier et al., 2006; Kharaka et al., 2006). These studies indicate that mineral carbonation will mainly occur by dissolution of Mg, Fe-silicates (and sulfides) and precipitation of Mg, Fe-carbonates (e.g. siderite, magnesite). In the Muderong Shale Mg and Fe are mainly present in pyrite, siderite and chlorite (Table 1). Here, siderite (2%) will have a neutral or negative balance, i.e. it might be dissolved near the CO_2–rock interface where pH is low but then precipitation will occur again when pH rises towards the top boundary of the sample plug. In case of siderite dissolution and non-precipitation a slight increase in sample porosity would be expected. Bertier et al. (2007) have shown that in a sandstone aquifer from the Campine Basin in Belgium dissolution of pyrite may occur. If the liberated iron becomes a source for the formation of siderite, then a slight decrease in sample porosity can be expected due to the lower density of siderite (~3.8 t/m^3) compared to pyrite (~5.0 t/m^3).

Chlorite is the predominant Mg/Fe-mineral in the Muderong Shale and might provide a significant source of these elements to form (Mg/Fe)-carbonates. If this occurred within the experimental timeframe and under the experimental conditions (*p*, *T*, pH) then a significant increase in sample

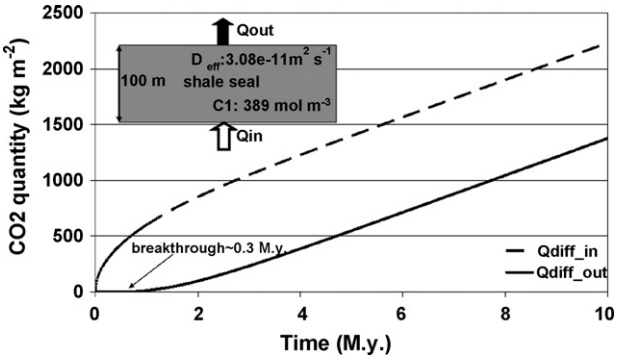

Fig. 13 – CO_2 diffusive loss through Muderong Shale, assuming cap rock thickness of 100 m and porosity of 20%.

porosity is reasonable, keeping in mind the different sample density of chlorite (~2.8 t/m^3) and magnesite/siderite (3.0–3.8 t/m^3). More detailed investigations on the influence of CO_2–water–rock interactions on sample properties (fluid flow behaviour, porosity, etc.) are planned in the future.

6. Diffusive loss through a cap rock

To assess the risk of diffusive CO_2 loss through a cap rock formation, the diffusion model of Krooss et al. (1992a,b) was used. For this evaluation, D_{eff} and C_1-values were taken from the results of diffusion Experiment 1 (Table 2). The following scenario was assumed: a cap rock thickness of 100 m at a reservoir depth of 1000 m (corresponding to temperatures of 45–50 °C and a fluid pressure of 10 MPa), porosity of 20% and an infinite source of pure CO_2 in the reservoir immediately underlying the cap rock. The governing equations are provided in Appendix (A5, A12). The resulting amounts of CO_2 entering the cap rock at the cap rock/reservoir interface and escaping from the top of the cap rock, respectively, are given in Fig. 13. For the parameters considered, diffusive gas breakthrough at the top boundary of the cap rock occurs after ~0.3 Ma. This time frame is considered reasonable for geological storage of CO_2, and for relatively thin shale (100 m). However, as geochemical alteration may occur owing to CO_2/water/rock interactions, the sealing integrity could be lower, leading to shorter diffusive breakthrough times.

7. Conclusion and outlook

The present study is, to our knowledge, the first investigation of the CO_2 sorption capacity of a fine-grained sedimentary rock and different clay minerals under conditions relevant for CO_2 subsurface storage (45–50 °C and pressures up to 20 MPa).

A combination of diffusion experiments and conventional gas sorption tests on the Muderong Shale from Western Australia has provided evidence for significant CO_2 storage capacity in shale sequences. The observed CO_2 fixation is attributed to a combination of aqueous solubility, geochemical reactions and physical sorption mainly on clay minerals. Sorption capacities, specifically for montmorillonite are high and of the same order of magnitude as natural coals.

The results of this study also indicate that geochemical alterations such as dissolution of silicates and precipitation of carbonates may have measurable effects on the porosity, permeability and diffusion properties of shales, with a tendency to enhance the transport properties. But even these enhanced transport properties are not likely to create substantial leakage problems through the undisturbed matrix of massive shale sequences. Indeed, by favouring the access to larger volumes of shale, they could positively contribute to mineral trapping of significant amounts of CO_2.

Considering the large proportions of shales that are present in sedimentary basins, there is significant CO_2 storage potential in such pelitic sequences. This sorption potential is, however, limited by the poor accessibility of low permeability lithotypes (e.g. shales, mudrocks). Thus, this retention capacity is an additional beneficial feature of low permeability shaly caprocks overlying potential underground CO_2 storage sites.

More detailed future studies are considered to be important for a more profound understanding of cap rock alteration resulting from interaction with carbon dioxide. These investigations could include repetitive diffusion experiments on the same sample plugs to detect long-term alterations caused by CO_2 interaction. Further, more detailed experimental studies on mineral alterations are suggested in order to obtain information on additional mineral CO_2 trapping as well as on possible alterations of porosity and permeability.

Acknowledgements

This study was conducted under the GEOTECHNOLOGIEN R&D-Programme funded by the German Ministry of Education and Research (BMBF) and the German Research Foundation (DFG) (publication no. GEOTECH-279, grant-nr. 03G0614A). Further, this work was supported through the APCRC Seals and GEODISC research programmes and their associated sponsors. Financial support is gratefully acknowledged.

Alexandra Amann and Stephen Guggenheim are thanked for their critical and thoughtful evaluation of the manuscript.

Appendix A. Evaluation of effective diffusion coefficients

Fick's first law of diffusion describes the diffusive flux rate, J_D [mass/(area time)], as a function of the concentration gradient (grad c; units: [mass/length^4]):

$$J_D = -D \operatorname{grad} c \tag{A1}$$

where D denotes the diffusion coefficient [length^2/time].

Fick's second law of diffusion is the mass balance equation:

$$\frac{\partial c}{\partial t} = D \frac{\partial^2 c}{\partial x^2} \tag{A2}$$

The definition of effective diffusion coefficients has been discussed previously in the literature (Krooss and Leythaeu-

ser, 1997). In this work the effective diffusion coefficient is defined as:

$$J_D = -D_{eff}\,\mathrm{grad}\,c_{bulk} \tag{A3}$$

Here D_{eff} denotes the effective diffusion coefficient [length^2/time] and c_{bulk} is the bulk concentration of the species under consideration in the (water-saturated) porous medium (mass per volume of bulk rock).

Gas diffusion through the rock samples under the experimental conditions can be described as non-stationary diffusion through a plane sheet. The concentration of the diffusing gas in the plane sheet as a function of distance (x) and time (t) is given by Crank (1975).

$$\begin{aligned} c = {} & c_1 + (c_2 - c_1)\frac{x}{l} \\ & + \frac{2}{\pi}\sum_{n=1}^{\infty}\frac{c_2\cos(n\pi) - c_1}{n}\sin\left(\frac{n\pi x}{l}\right)e^{-Dn^2\pi^2 t/l^2} \\ & + \frac{4c_0}{\pi}\sum_{m=1}^{\infty}\frac{1}{2m+1}\sin\left(\frac{(2m+1)\pi x}{l}\right)e^{-D(2m+1)^2\pi^2 t/l^2} \end{aligned} \tag{A4}$$

c_1 is the concentration within the plane sheet at the boundary $x = 0$ (plane sheet/gas phase interface), c_2 the concentration within the plane sheet at the boundary $x = l$ (top of plane sheet with length l), c_0 the initial concentration throughout the plane sheet.

Inserting Eq. (A4) into Eq. (A2) and integrating over time yields the cumulative amount Q_{out} of gas that has passed through the plane sheet at time t:

$$\begin{aligned} Q_{out} = {} & D(c_1 - c_2)\frac{t}{l} + \frac{2l}{\pi^2}\sum_{n=1}^{\infty}\frac{c_1\cos(n\pi) - c_2}{n^2}\left[1 - e^{-Dn^2\pi^2 t/l^2}\right] \\ & + \frac{4c_0 l}{\pi^2}\sum_{m=0}^{\infty}\frac{1}{(2m+1)^2}\left[1 - e^{-D(2m+1)^2\pi^2 t/l^2}\right] \end{aligned} \tag{A5}$$

With the boundary conditions $c_0 = 0$, c_1 = constant ($x = 0$ and $t \geq 0$) and $c_2 = 0$ ($x = l$ and $t \geq 0$) Eq. (A5) simplifies to

$$\frac{Q_{out}}{lc_1} = \frac{Dt}{l^2} - \frac{1}{6} - \frac{2}{\pi^2}\sum_{n=1}^{\infty}\frac{(-1)^n}{n^2}e^{-Dn^2\pi^2 t/l^2} \tag{A6}$$

and for $t \to \infty$

$$\frac{Q(t)}{lc_1} = \frac{Dt}{l^2} - \frac{1}{6} \tag{A7}$$

Rearranging Eq. (A7) gives

$$Q(t) = \frac{c_1 Dt}{l} + Q_0 \tag{A8}$$

with

$$Q_0 = -\frac{lc_1}{6} \quad [\mathrm{mol\,m^{-2}}] \tag{A9}$$

and

$$t_0 = -\frac{Q_0 l}{c_1 D} = \frac{l^2}{6D} \tag{A10}$$

where t_0 is denoted as lag time (Krooss and Schäfer, 1987).

For the evaluation of the diffusion experiments, Eq. (A11) is fitted to the experimental $Q(t)$ values by means of a least-squares procedure and variation of the parameters Q_0 and t_0

$$Q(t) = Q_0\left(1 - \frac{t}{t_0} + \frac{12}{\pi^2}\sum_{n=1}^{\infty}\frac{(-1)^n}{n^2}e^{-n^2\pi^2 t/6t_0}\right) \tag{A11}$$

In the corresponding expression for Eq. (A6), the amount of diffusing substance that has entered the cap rock from the reservoir is given as follows:

$$\frac{Q_{in}}{lc_1} = \frac{Dt}{l^2} + \frac{2}{\pi^2}\sum_{n=1}^{\infty}\frac{1}{n^2}\left(1 - e^{-Dn^2\pi^2 t/l^2}\right) \tag{A12}$$

REFERENCES

Al-Basali, T.M., Zhang, J., Sharma, M.M., 2005. Measurement of the sealing capacity of shale caprocks. In: SPE Annual Technology Conference and Exhibition, Houston, Texas, October 9–12 (SPE 96100).

Bachu, S., 2000. Sequestration of CO_2 in geological media: criteria and approach for site selection in response to climate change. Energy Convers. Manage. 41, 953–970.

Bachu, S., Gunter, W.D., Perkins, E.H., 1994. Aquifer disposal of CO_2: hydrodynamic and mineral trapping. Energy Convers. Manage. 35, 269–279.

Bertier, P., Swennen, R., Laenen, B., Lagrou, D., Dreesen, R., 2006. Experimental identification of CO_2–water–rock interactions caused by sequestration of CO_2 in Westphalian and Buntsandstein sandstones of the Campine Basin (NE-Belgium). J. Geochem. Explor. 89, 10–14.

Bertier, P., Swennen, R., Laenen, B., 2007. Evaluation of the CO_2-sequestration capacity of sandstone aquifers in the Campine Basin (NE-Belgium) based on autoclave experiments and numerical modelling. In: Goldschmidt 2007, August 20–24, Cologne, Germany.

Brosse, E., 2005a. Special Issue—IFP International Workshop "Gas–Water–Rock Interactions Induced by Reservoir Exploitation, CO_2 Sequestration, and other Geological Storage". Oil & Gas Science and Technology—Revue de l'Institut Français du Pétrole 60, pp. 1–206.

Brosse, E., 2005b. Special Issue—IFP International Workshop "Gas–Water–Rock Interactions Induced by Reservoir Exploitation, CO_2 Sequestration, and Other Geological Storage". Oil & Gas Science and Technology—Revue de l'Institut Français du Pétrole 60, pp. 207–433.

Busch, A., Gensterblum, Y., Krooss, B.M., 2003. Methane and CO_2 sorption and desorption measurements on dry Argonne Premium Coals: pure components and mixtures. Int. J. Coal Geol. 55, 205–224.

Brunauer, S., Emmett, P.H., Teller, E., 1938. Adsorption of gases in multimolecular layers. J. Am. Chem. Soc. 60, 309–319.

Busch, A., Gensterblum, Y., Krooss, B.M., Littke, R., 2004. Methane and carbon dioxide adsorption/diffusion

experiments on coal: an upscaling- and modelling approach. Int. J. Coal Geol. 60, 151–168.
Busch, A., Gensterblum, Y., Krooss, B.M., Siemons, N., 2007. Investigation of high-pressure selective adsorption/desorption behaviour of CO_2 and CH_4 on coals: an experimental study. Int. J. Coal Geol. 66, 53–68.
Chiquet, P., Broseta, D., Thibeau, S., 2005. Capillary alteration of shaly caprocks by carbon dioxide. In: SPE Europec/EAGE Annual Conference (SPE 94183), June 13–16, Madrid, Spain.
Chlou, C.T., Rutherford, D.W., 1993. Sorption of N1 and EGME vapors on some soils, clays, and mineral oxides and determination of sample surface areas by use of sorption data. Environ. Sci. Technol. 27, 1587–1594.
Costanzo, P.M., Guggenheim, S., 2001. Baseline studies of the clay minerals society source clays. Clay Clay Miner. 49, 371–454.
Crank, J., 1975. The Mathematics of Diffusion, second ed. Oxford University Press.
Dewhurst, D.N., Jones, R.M., Raven, M.D., 2002a. Microstructural and petrophysical characterisation of Muderong Shale: application to top seal risking. Petrol. Geosci. 8, 371–383.
Dewhurst, D.N., Raven, M.D., van Ruth, P., Tingate, P.R., Siggins, A.F., 2002b. Acoustic properties of Muderong Shale. APPEA J. 42, 241–257.
Dewhurst, D.N., Hennig, A., 2003. Geomechanical properties related to top seal leakage in the Carnarvon Basin, Northwest Shelf, Australia. Petrol. Geosci. 9, 255–263.
Duan, Z., Sun, R., 2003. An improved model calculating CO_2 solubility in pure water and aqueous NaCl solutions from 273 to 533 K and from 0 to 2000 bar. Chem. Geol. 193, 257–271.
Emberley, S., Hutcheon, I., Shevalier, M., Durocher, K., Gunter, W.D., Perkins, E.H., 2004. Geochemical monitoring of fluid–rock interaction and CO_2 storage at the Weyburn CO_2-injection enhanced oil recovery site, Saskatchewan, Canada. Energy 29, 1393–1401.
Freund, P., Ormerod, W.G., 1997. Progress toward storage of carbon dioxide. Energy Convers. Manage. 38, 199–2004.
Gaus, I., Azaroual, M., Czernichowski-Lauriol, I., 2005. Reactive transport modelling of the impact of CO_2 injection on the clayey cap rock at Sleipner (North Sea). Chem. Geol. 217, 319–337.
Gertz, K.H., Loeschcke, H.H., 1956. Bestimmung des Diffusionskoeffizienten von CO_2 in Wasser [Determination of the diffusion coefficient of CO_2 in water]. Zeitschrift für Naturforschung 11b, 61–64.
Gunter, W.D., Perkins, E.H., McCann, T.J., 1993. Aquifer disposal of CO_2-rich gases: reaction design for added capacity. Energy Convers. Manage. 34, 941–948.
Gunter, W.D., Perkins, E.H., Hutcheon, I., 2000. Aquifer disposal of acid gases: modelling of water–rock reactions for trapping of acid wastes. Appl. Geochem. 15, 1085–1095.
Hildenbrand, A., Schlömer, S., Krooss, B.M., Littke, R., 2004. Gas breakthrough experiments on pelitic rocks: comparative study with N_2, CO_2 and CH_4. Geofluids 4, 61–80.
Hitchon, B., Gunter, W.D., Gentzis, T., Bailey, R.T., 1999. Sedimentary basins and greenhouse gases: a serendipitous association. Energy Convers. Manage. 40, 825–843.
Holloway, S., 1997. Safety of the underground disposal of carbon dioxide. Energy Convers. Manage. 38, 241–245.
Kaszuba, J.P., Janecky, D.R., Snow, M.G., 2003. Carbon dioxide reaction processes in a model brine aquifer at 200 °C and 200 bars: implications for geologic sequestration of carbon. Appl. Geochem. 18, 1065–1080.
Kaszuba, J.P., Janecky, D.R., Snow, M.G., 2005. Experimental evaluation of mixed fluid reactions between supercritical carbon dioxide and NaCl brine: relevance to the integrity of a geologic carbon repository. Chem. Geol. 217, 277–293.
Kharaka, Y.K., Cole, D.R., Thordsen, J.J., Kakouros, E., Nance, H.S., 2006. Gas–water–rock interactions in sedimentary basins: CO_2 sequestration in the Frio formation, Texas, USA. J. Geochem. Explor. 89, 183–186.
Knauss, K.G., Johnson, J.W., Steefel, C.I., 2005. Evaluation of the impact of CO_2, co-contaminant gas, aqueous fluid and reservoir rock interactions on the geologic sequestration of CO_2. Chem. Geol. 217, 339–350.
Kovack, G.E., Dewhurst, D.N., Raven, M.D., Kaldi, J.G., 2004. The influence of composition, diagenesis and compaction on seal capacity in the Muderong Shale, Carnarvon Basin. APPEA J. 44, 201–222.
Krooss, B.M., Schäfer, R.G., 1987. Experimental measurements of the diffusion parameters of light hydrocarbons in water-saturated sedimentary rocks. I. A new experimental procedure. Org. Geochem. 11, 193–199.
Krooss, B.M., Leythaeuser, D., 1988. Experimental measurements of the diffusion parameters of light hydrocarbons in water-saturated sedimentary rocks. II. Results and geochemical significance. Org. Geochem. 12, 91–108.
Krooss, B.M., Leythaeuser, D., Schäfer, R.G., 1992a. The quantification of diffusive hydrocarbon losses through cap rocks of natural gas reservoirs—a re-evaluation. AAPG Bull. 76, 403–406.
Krooss, B.M., Leythaeuser, D., Schäfer, R.G., 1992b. The quantification of diffusive hydrocarbon losses through cap rocks of natural gas reservoirs—a re-evaluation: reply. AAPG Bull. 76, 1842–1846.
Krooss, B.M., Leythaeuser, D., 1996. Molecular diffusion of light hydrocarbons in sedimentary rocks and its role in migration and dissipation of natural gas. AAPG Memoir, vol. 66. pp. 173–181.
Krooss, B.M., Leythaeuser, D., 1997. Diffusion of methane and ethane through the reservoir cap rock; implications for the timing and duration of catagenesis; discussion. AAPG Bull. 81, 155–161.
Krooss, B.M., van Bergen, F., Gensterblum, Y., Siemons, N., Pagnier, H.J.M., David, P., 2002. High-pressure methane and carbon dioxide adsorption on dry and moisture-equilibrated Pennsylvanian coals. Int. J. Coal Geol. 51, 69–92.
Krooss, B.M., Busch, A., Alles, S., Hildenbrand, A., 2003. Experimental investigation of molecular diffusion of CO_2 in coals and shales. In: International Conference on Gas–Water–Rock Interactions Induced by Reservoir Exploitation, CO_2 Sequestration, and other Geological Storage, November 18–20, Rueil-Malmaison, France.
Leythaeuser, D., Schäfer, R.G., Yükler, A., 1980. Diffusion of light hydrocarbons through near-surface rocks. Nature 284, 522–525.
Montel, F., Caillet, G., Pucheu, A., Caltagirone, J.P., 1993. Diffusion model for predicting reservoir gas losses. Marine Petrol. Geol. 10, 51–57.
Melnitchenko, A., Thompson, J.G., Volzone, C., Ortiga, J., 2000. Selective gas adsorption by metal exchanged amorphous kaolinite derivatives. Appl. Clay Sci. 17, 35–53.
Nelson, J.S., Simmons, E.S., 1992. The quantification of diffusive hydrocarbon losses through cap rocks of natural gas reservoirs—a re-evaluation: discussion. AAPG Bull. 76, 1839–1841.
Nelson, J.S., Simmons, E.S., 1995. Diffusion of methane and ethane through the reservoirs cap rock: implications for the timing and duration of catagenesis. AAPG Bull. 79, 1064–1074.
Nuttall, B.C., Eble, C.F., Drahovzal, J.A., Bustin, R.M., 2005. Analysis of Devonian black shales in Kentucky for potential carbon dioxide sequestration and enhanced natural gas production. Report Kentucky Geological Survey/University of Kentucky (DE-FC26-02NT41442).

Rosenbauer, R.J., Koksalan, T., Palandri, J.L., 2005. Experimental investigation of CO_2–brine–rock interactions at elevated temperature and pressure: implications for CO_2 sequestration in deep-saline aquifers. Fuel Process. Technol. 86, 1581–1597.

Schlömer, S., Krooss, B.M., 2004. Molecular transport of methane, ethane and nitrogen and the influence of diffusion on the chemical and isotopic composition of natural gas accumulations. Geofluids 4, 81–108.

Siemons, N., Busch, A., 2007. Measurement and interpretation of supercritical CO_2 adsorption on worldwide coals. Int. J. Coal Geol. 69, 229–242.

Shiraki, R., Dunn, T.L., 2000. Experimental study on water–rock interactions during CO_2 flooding in the Tensleep Formation, Wyoming, USA. Appl. Geochem. 15, 265–279.

Venaruzzo, J.L., Volzone, C., Rueda, M.L., Ortiga, J., 2002. Modified bentonitic clay minerals as adsorbents of CO, CO_2 and SO_2 gases. Micropor. Mesopor. Mater. 56, 73–80.

Vivian, J.E., King, C.J., 1964. Diffusivities of slightly soluble gases in water. AICHE J. 10, 220–221.

Volzone, C., Ortiga, J., 2000. O_2, CH_4 and CO_2 gas retentions by acid smectites before and after thermal treatment. J. Mater. Sci. 35, 5291–5294.

Volzone, C., Rinaldi, J.O., Ortiga, J., 2002. N_2 and CO_2 adsorption by TMA- and HDP-montmorillonites. Mater. Res. 5, 475–479.

Volzone, C., Ortiga, J., 2006. Removal of gases by thermal-acid leached kaolinitic clays: influence of mineralogical composition. Appl. Clay Sci. 32, 87–93.

Volzone, C., Rinaldi, J.O., Ortiga, J., 2006. Retention of gases by hexadecyltrimethylammonium–montmorillonite clays. J. Environ. Manage. 79, 247–252.

Zhang, T., Krooss, B.M., 2001. Experimental investigation on the carbon isotope fractionation of methane during gas migration by diffusion through sedimentary rocks at elevated temperature and pressure. Geochim. Cosmochim. Acta 65, 2723–2742.